Experimental investigation of power capture from pitching point absorbers

F. Flocard[1] and T.D. Finnigan[2]

[1] School of Civil Engineering,
The University of Sydney,
NSW 2006 Sydney, Australia
E-mail: f.flocard@civil.usyd.edu.au

[2] Biopower Systems Pty. Ltd.,
Australian Technology Park,
NSW 1430 Eveleigh, Australia
E-mail: tfinnigan@biopowersystems.com

Abstract

This paper presents results from an experimental study on the power capture of bottom-pivoted pitching point absorbers in intermediate water depth subjected to regular and irregular waves. The present research investigates the respective influence of parameters such as geometry, damping and inertia modification (ballasting) on the performance of bottom-pivoted pitching wave energy converters in realistic sea states. Results indicate that this type of wave energy device performs best in moderate sea states, although the net power output would be greater in larger sea states. The pitch displacement angle, relative to vertical, is typically less than +/-15° under normal operation. The two most influential parameters, damping and ballasting, have a dramatic influence on the performance of the device. Moreover, it is shown that these parameters can be adjusted in response to the wave conditions to optimise power capture. From the results of the experiments in irregular waves, a full scale cylinder-shaped prototype of 6m diameter located in 25m water depth could absorb approximately 130 kW (average) in nominal winter conditions (based on observations from the North Atlantic) and approximately 40 kW (average) in summer sea states.

Keywords: Experimental, Pitch, Point–absorbers, Wave Energy

Nomenclature

a_i	= amplitude of regular wave
c_f	= capture factor
c_{fv}	= capture volume factor
c_d	= hydrodynamic linear drag damping component
c_r	= radiation damping coefficient
c_{PTO}	= PTO damping coefficient
ζ	= water surface elevation
D	= Diameter/width of the cylinder
f_i	= frequency of regular wave
H_s	= significant wave height
KC	= Keulegan Carpenter Number
λ	= incident wavelength
λ_c	= capture width
P_{PTO}	= power captured
P_i	= incident wave power
T_e	= energy period
θ	= pitch displacement angle

1 Introduction

As for the oil crisis in 1970s, the increased concern for global warming we have witnessed these last years has been an incredible stimulant for the advancement of alternative energies sources such as marine energies. However, in these times of worldwide economic crisis and in order to be successful in their development, wave energy conversion technologies must be commercially viable.

Therefore, the devices must be small as they could then be deployed in arrays in wave farms (as for wind turbines), reducing the production costs, increasing the flexibility and reliability of such a plant.

Wave energy devices can be classified according to their location as either: offshore, nearshore or shoreline. The devices presented in this paper belong to the nearshore category (approximately 25m water-depth and a maximum of 2.5km for the coast) as they present numerous advantages. Despite the fact that energy levels are higher in deep water offshore locations, its beneficial from a design point a view to have the devices in nearshore intermediate water depths, as they are protected from the extreme forces developed in storms, the high energetic seas being dissipated due to natural wave breaking, and as installation and maintenance costs are greatly reduced. The visual and environmental impacts are lower than for shoreline devices, increasing the positive perception from the local population, moreover this location has a higher annual average incident wave power than directly on the shore where a lot of energy dissipation takes place due to bottom friction and wave breaking.

Finally, it is of the utmost importance that the device is able to survive in storms. The choice of a bottom fixed pitching device has a clear advantage as it offers the possibility to “sink” the device when a storm approaches, having it lay near the bottom in calm waters, and then bring back into working position once it is considered to be safe again. This presents the opportunity to structurally design a device that only needs to withstand the loads from waves up to a certain height as it can be naturally protected from the stormy and dangerous seas in which case it would also not be able to extract power due to generator limitations.

This paper begins by describing the conversion principle of small pitching Wave Energy Converters (WEC). A brief presentation of the experimental arrangement and of the different wave conditions is then given. Finally, the power capture of the cylinders is investigated experimentally through a parametric study on the geometry, the inertia and the Power Take Off (PTO) damping. Moreover, the possibility of studying different geometries will give information on the respective influence of viscous drag and radiation damping.

2 Analysis of pitching point absorbers

The wave energy converters investigated in this study are of the resonant Point Absorber (PA) type, which can be defined as a buoyant body with dimensions that are small in comparison to the incident wavelength. This conversion principle was first studied in the seventies by Budal and Falnes [1] and by Evans [2], for heaving and swaying bodies. They showed that such devices could absorb energy from a greater width than their physical dimension. Falnes [3] used an electrical analogy to explain this phenomenon, as the floating body acts like electrical dipole, with the radiated waves it generates interacting destructively with the incident waves

The equation of motion for such a WEC can be expressed under the following form (Caska and Finnigan[4]) with the assumptions that the incident waves are harmonic and linear:

$$[I + I_a]\ddot{\theta} + (c_r + c_d + c_{PTO})\dot{\theta} + K\theta = M_I + M_D \qquad (2.1)$$

where I is the moment of inertia of the structure, I_a is the frequency dependent added mass moment of inertia, c_r is the radiation damping coefficient, c_d is the hydrodynamic viscous drag damping component, c_{PTO} is the PTO damping coefficient and $K\theta$ is the restoring moment due to buoyancy. M_I and M_D are respectively the inertial and drag moment exciting the WEC as defined in the Morison’s equation. The equation (2.1) is included here only for reference and it should be noted that the experiments presented below do not strictly adhere to the required conditions, as the studied waves extend to non-linear regimes.

3 Experimental arrangement

Wave flume

The experiments were conducted in the University of Sydney wave flume. The flume is 30 meters long, 1.0 meters wide and a 0.75m still water depth was used for the experiments. Waves were generated by an Edinburgh Designs wave maker.

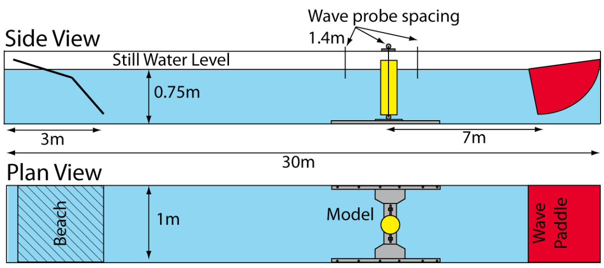

Figure 1: Wave flume arrangement

A Froude scaling ratio of 1/33 was used to relate the wave flume water depth of 0.75m to a typical prototype mean water level of 25m.

Using Froude scaling has a clear limitation, as it does not allow for a correct scaling of viscous effects such as drag. However, the damping due to viscous drag at model scale is expected to be greater than at prototype scale, as the Reynolds number for the model is lower than for the prototype, and power capture from the experiments can be then considered to be conservative. This is also applicable to the study of the influence of vortices generated in the highest and longest waves. This effect could be beneficial for energy dissipation in powerful seas but should be investigated further as it may also result in large dynamic loads on the structures.

Test Rig

The experimental rig consists of two main parts. Firstly, the underwater rotating shaft on which are mounted the different cylinders to be tested (see Fig. 2). The cylinders each have a distinct compartment at the top which can be filled in order to test the effect of changing the inertia and therefore simulate the effect, at prototype scale, of allowing water to fill some portion of the cylinder (i.e. water ballasting).

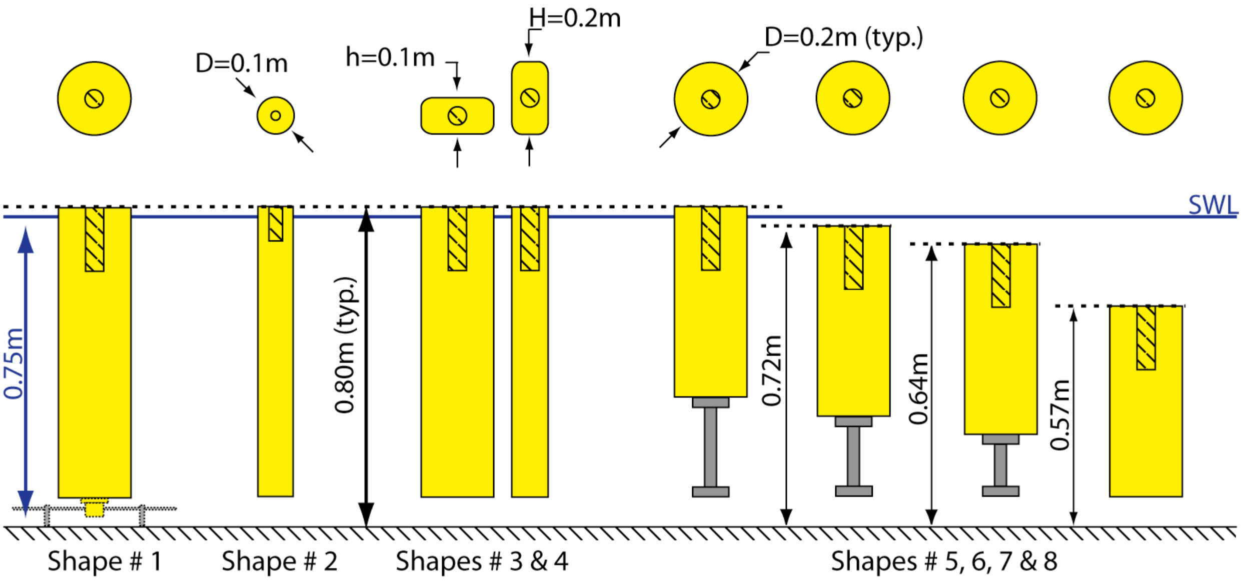

Figure 2: The different cylinders tested

Therefore, for all the tests mentioned in this paper, "Ballasted" (**B**) will mean that the compartment is filled (with lead), and "Not Ballasted" (**No B**) that the compartment is left empty. The rig is bolted to stainless steel rails fixed to the wave tank walls in order to ensure that it is well aligned with wave direction.

As recommended by Chakrabati [5], the dimensions of the widest shapes tested do not exceed 1/5th of the tank width. Despite following this rule, it is clear that reflection of the radiated waves will have an influence on the power captured by the different shapes and is not fully representative of their performance in real ocean conditions.

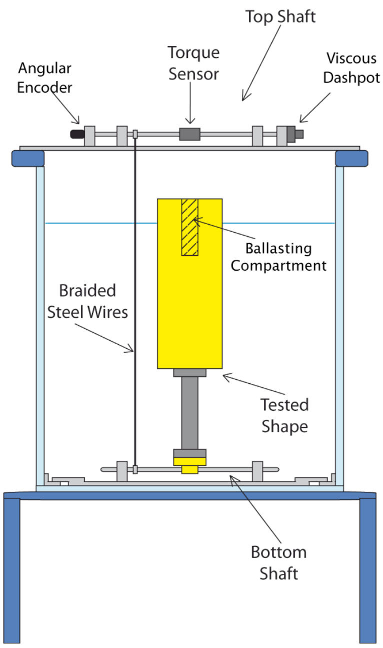

Figure 3: Layout of experimental rig

Secondly, another rotating shaft on which is mounted the sensor suite is located above the water on the top of the wave tank. This has the clear advantage of having all the sensors accessible and out of the water. The two rotating shafts are coupled through thin pre-tensioned stainless steel wires and thus it is possible to measure the torque applied by the tested cylinder against the viscous dashpot representing the Power Take-Off by use of the dynamometer.

The damping coefficient, c_{PTO}, can be set over the range 0.1–12 Nms/rad. However, in most of the experiments presented in the following sections, c_{PTO} was set to a value of 10 Nms/rad, as it was suitable for Shapes #1, 3 & 5. Consequently, PTO damping was not tuned and optimised for each and every configuration and the resulting power output not maximised. This restriction is clearly unfavourable for certain configurations presented here and will be more thoroughly studied for optimum cases in the future.

The dynamometer consists of a low-friction rotary encoder, a reaction torque sensor mounted floating on the shaft in order to only record the torque against the rotary dashpot which acts as a linear damper, as would behave a hydraulic machine or a direct drive generator.

From equation (2.1), it is possible to express the effective power absorbed by the WEC and converted through the PTO by:

$$P(t) = c_{PTO}\,\dot{\theta}(t)^2 \tag{3.1}$$

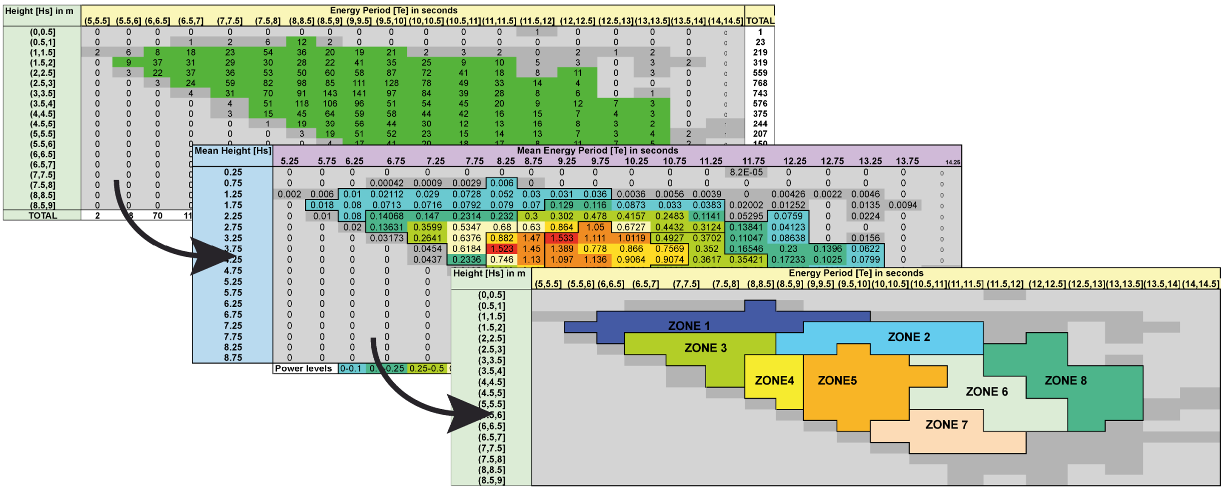

Figure 4: Subdivision of the Winter scatter table in 8 wave climate zones

Therefore, in the case of our experiments, the instantaneous power absorbed by the cylinder is obtained through the measurements of the reaction torque sensor (T) and the angular encoder (θ) and is given by:

$$P(t) = T\dot{\theta}(t) \qquad (3.2)$$

Mechanical friction in the system can be considered as negligible when compared to hydrodynamics and dashpot damping.

Three wave gauges were located around the device to measure the wave elevations and the influence of the device when pitching.

4 Wave Climate

Regular Waves

The first sets of experiments were conducted in regular waves with model frequencies from 0.42 Hz to 0.96 Hz. This corresponds to full-scale wave periods from 6s to 14s. The wave amplitudes generated by the paddle were 1.5, 3.0, 4.5 and 6.0 cm corresponding to full-scale waves of approximately 1, 2, 3 and 4 m height. These regular waves can all be described as intermediate water depth waves and range from weakly non-linear to Stokes 2nd order wave regimes. These conditions span the range across which a WEC can be expected to be productive when deployed in the ocean.

Irregular Waves

It is of great importance to study the behaviour and the power output of wave energy devices in irregular wave fields as they better represent the real ocean conditions. Moreover, it is useful to test the canonical structures in realistic wave climates that have been experienced by existing devices.

The combined use of European Marine Energy Centre (EMEC) scatter tables and Bretschneider spectra allow the generation of realistic wave conditions and power capture predictions.

Bretschneider spectra are widely used throughout the ocean wave energy community (Saulnier et al [6], Meadowcroft et al [7]) and are in a good agreement with the prevalent wind waves conditions found in the North Sea. It is defined by the following formula:

$$S_B(f) = 5\frac{m_0}{f_p}\left(\frac{f_p}{f}\right)^5 e^{-\frac{5}{4}\left(\frac{f_p}{f}\right)^4} \qquad (4.1)$$

Data obtained from the EMEC consisted of twelve scatter tables for 11 months of the year 2006 and January 2007. The data from October 2006 were not available.

After analysis of the yearly data, it was decided to create two different wave climates, one very energetic, called Winter and consisting of the three most energetic consecutive months (November 2006, December 2006 and January 2007); and another called Summer, less energetic, consisting of May, June and July 2006.

It was then necessary to simplify these tables in order to be able to reproduce their information during wave tank simulation by having a feasible number of tests.

This was achieved by conducting a zonation on the scatter table and create bigger cells, each with its own (H_s, T_e) characteristics, such as in the scatter table in Fig. 4, where the whole table is then summarized by 8 different zones with different characteristics. The selection of the different zones was based on the power levels (using the formulas recommended by Pitt [8]) of the cells and their frequency of occurrence.

This solution enables us to still have a reasonable representation of the EMEC wave climate by reducing the number of tests while being able to analyse the behaviour of the device in very different wave climate conditions.

Zone #	Winter H_s (m)	Winter T_e (s)	Winter Occ. (%)	Summer H_s (m)	Summer T_e (s)	Summer Occ. (%)
1	1.5	7.6	9.8	0.3	4.5	8.2
2	2.2	10.1	19.1	0.5	8.3	7.4
3	2.9	7.5	14.2	1.5	5.8	12.5
4	4.1	8.5	15.2	1.7	6.8	37.1
5	4.5	9.8	29.4	1.6	8.1	23.3
6	4.9	11.5	5.8	2.5	8.9	7.1
7	6.6	11.0	3.6	2	10.9	2.9
8	4.2	12.6	2.9	3.6	10.2	1.5

Table 1: Sea-states characteristics (full-scale) used for the tests

This allowed us to test in a range of very diverse wave conditions, and in the case of the Zone 7 of Winter, have some first results on the behaviour of the device in such powerful seas we could expect the device to face during storms.

5 Results

Power absorption in regular waves

PTO Damping

A first test series was performed on the different shapes in order to determine the best PTO damping coefficient ($c_{PTOopt.}$) for our range of regular wave conditions. It was clear from these tests (see Fig. 5) that under-damping (c_{PTO1}) the device resulted in reduced power captured. The gain from a high damping value (c_{PTO2}) was only visible in the highest waves with longer periods, which are not occurring very frequently.

The reason for this trend is due to the fact that power captured is the product of angular velocity and damping torque. A low damping coefficient will result in high angular velocity but small torque, while a high damping coefficient results in high torque but reduced angular velocity. A compromise must be found for the best power capture possible. Such "tuning" of the performance was not included in this study, and therefore the performance could be considered generally sub-optimal. Nevertheless, the limited number of damping settings used did show distinct performance differences, suggesting the relative effect of damping.

The influence of the PTO damping was also noticeable on the maximum pitching angles achieved by the different shapes as it rarely went above 15°, even around resonance in waves of a_i = 0.06m (see Fig. 6) and with low damping coefficient for c_{PTO1} and c_{PTO2}.

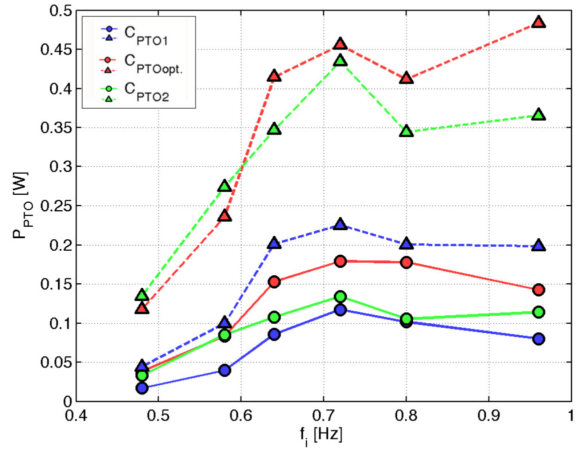

Figure 5: Power captured for Shape#7 NoB in regular waves a_i = 0.03m (▲) and a_i = 0.045m (●)

Positive pitch is defined as the downstream direction (towards the beach) whereas negative pitch is in the upstream direction (towards the wave paddle). As expected, the pitch angles increase with a decrease in PTO damping and an increase in wave amplitude.

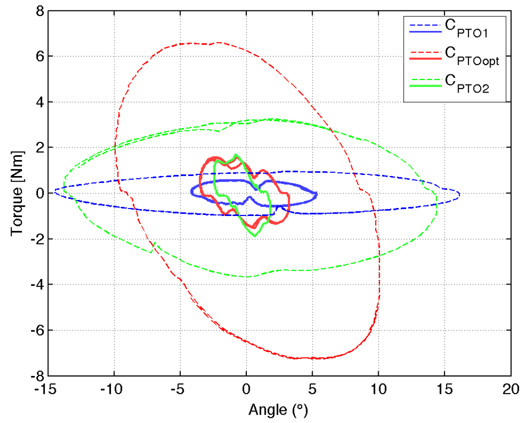

Figure 6: Work cycle for Shape#7 NoB a_i = 0.03m (—) and Shape#5 NoB a_i = 0.06m (...)

They are at a maximum in the vicinity of natural frequency where resonance occurs. An asymmetry of the pitch can also be observed, with pitch being more positive at resonance and for higher frequencies. This characteristic of the pitch, for bottom pivoted vertical cylinders, due to convective effects has also been found in a non-linear numerical model by Caska and Finnigan [4].

Geometry

A common way to measure the efficiency of a WEC is the capture factor c_f, defined as the ratio of capture width $\lambda_c = P_{PTO}/P_i$, where P_{PTO} is the power absorbed by the device and P_i is the incident wave power per unit width, by the physical width of the device.

$$c_f = \frac{P_{PTO}}{P_i D} \tag{5.1}$$

The second test series focused on the influence of the different geometries. The Shape#1 was used as a reference as it presents the largest volume due to its large width and height. Its capacity to act as a good wave maker was observed during pluck tests in still water (its natural frequency f_n = 0.59Hz when unballasted, i.e. **No B**, which is equivalent to a prototype natural period T_p = 10s), as an important radiated wave was generated. This was confirmed during the regular wave tests (see Fig.8) as the Point Absorber effect is apparent in moderate wave heights, with capture factor close to $c_f = 1$. The importance of the cylinder to be a good wave maker in order to be an efficient wave absorber was also proved with the poor performance of Shape#2 as its maximum c_f was lower than 0.5.

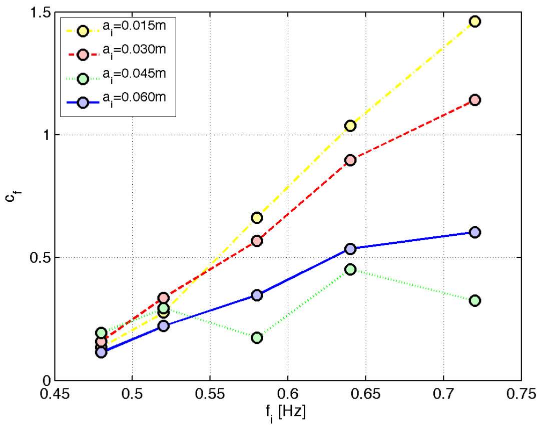

Figure 7: c_f for Shape#1 NoB in regular waves

The greatest performance is found for the smallest sea states, as viscous losses are smaller in small amplitude waves due to smaller Keulegan-Carpenter number (*KC*) of the upper part of the cylinder, which increases with wave height causing the viscous drag damping coefficient c_d to increase as well. Therefore, smaller wave conditions allow for the ideal linear conditions of the PA theory. More power can be extracted at larger wave heights but at a lower efficiency. This trend has been previously illustrated in other WEC devices such as the WRASPA (Chaplin & Aggidis[9]) and studies from Vantorre et al [10] and Folley et al [11].

Shape#1 and Shape#3 (f_n = 0.55 Hz) were then compared with a common PTO setting in order to judge the difference of a less streamlined shape in intermediate water depth. The same trend in power captured was observed for both shapes in intermediate and large wave height (see Fig.8) but with a better performance for Shape#1, as vortices around the edges of Shape #3 were observed over a broad range of wave conditions, resulting in undesirable energy dissipation.

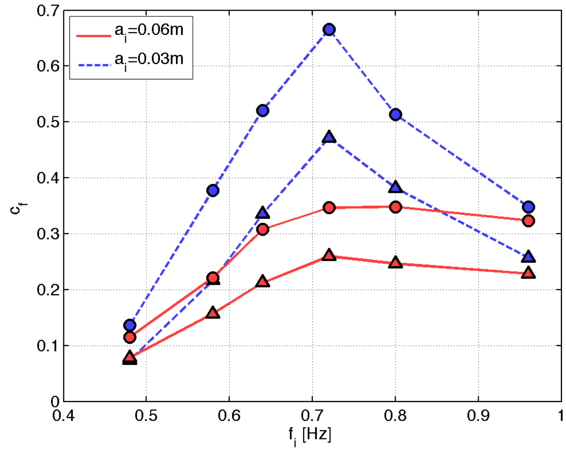

Figure 8: Comparison of c_f for Shapes #1(●) & #3 (▲) NoB in regular waves (a_i = 0.06m a_i = 0.03m)

The decrease in performance of the cylinders for bigger waves at low frequencies is mostly due to energy dissipation in vortex shedding, as *KC* tends to increase for waves of longer period and bigger amplitude and cause the c_d to increase. This has been clearly visualised in the wave flume and could act as a protection mechanism for the WEC in powerful sea conditions.

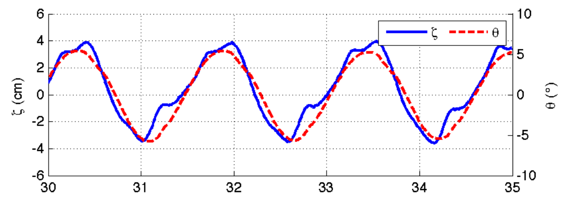

Figure 9: Surface elevation and pitching angle versus time for Shape#1 No B in regular wave (a_i = 0.03m, f_i = 0.64Hz)

For higher wave frequencies, the reason for the lower c_f is that the cylinder tends to be decoupled from the waves. This is illustrated on Fig.9 & 10, for Shape#1, at two different frequencies, one close to the resonance and one at the higher end of the tested range.

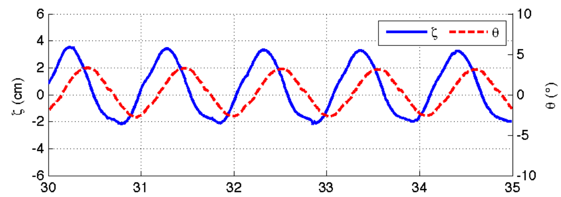

Figure 10: Surface elevation and pitching angle versus time for Shape#1 No B in regular wave (a_i = 0.03m, f_i = 0.96Hz)

The comparison of Shape#1 with Shape#5 (see Fig. 11) confirmed the fact the lower section of the cylinder (30% of the total volume) of Shape#1 had no beneficial influence on power capture in the water depth investigated. It also highlights the limitation of a comparison based solely on c_f as it doesn't take in account the important change in volume of the device and will be further addressed in the next section.

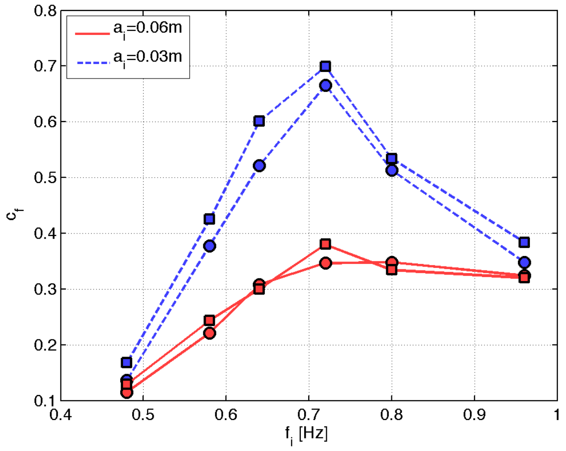

Figure 11: Comparison of c_f for Shapes #1(●) & #5 (■) NoB in regular waves (a_i = 0.06m a_i = 0.03m)

One last geometric parameter investigated was the vertical position of the cylinder relative to the water surface. This was performed by comparing the respective power capture performance of the Shapes#5, 6, 7 & 8 all of which are composed of the same cylinder mounted on different extensions. They were all tested with a common PTO setting causing Shapes#7 & 8 to be over constrained for the smallest waves.

Shape #	h_{top} model (m)	h_{top} prototype (m)
5	+ 0.05	+ 1.7
6	- 0.03	- 1.0
7	- 0.09	- 3.0
8	- 0.18	- 6.0

Table 2: h_{top} model & prototype for the Shapes#5, 6, 7 & 8

The location of the top of the different shapes in regard to mean water level (h_{top}) is given in the following table, with the scaled up equivalent for a full-scale prototype in 25m water depth. Using Shape#5 as a reference, the resulting power loss for the different shapes due to a decrease in h_{top} was very important (see Table 3) even for the smallest difference in location of the top of the cylinder.

Shape #	a_i = 0.015 (m)	a_i = 0.03 (m)	a_i = 0.045 (m)	a_i = 0.06 (m)
6	-87%	-56%	-42%	-24%
7	-100%	-81%	-65%	-53%
8	-100%	-98%	-91%	-81%

Table 3: Difference in power captured with Shape#5 for the Shapes#6, 7 & 8

This is an important feature to study, as it is desirable to design a device, which is not obstructive to the users of the sea and with minimum visual impact for a good reception from the public. It is a challenge to satisfy these conditions as wave energy decreases rapidly with depth and some locations can experiment water surface differences of a couple meters due to the influence of tides.

Ballasting

The third test series focused on the influence of ballasting on power capture for the different shapes at a constant damping rate of $c_{PTOopt.}$ = 10Nms/rad. This was performed by adding a mass of lead shot in the ballasting compartment (see Fig. 3) and the results are presented in Fig.12 for Shape#1. With the supplementary mass of 0.950kg (**B**), the natural frequency decreases to f_n = 0.52 Hz.

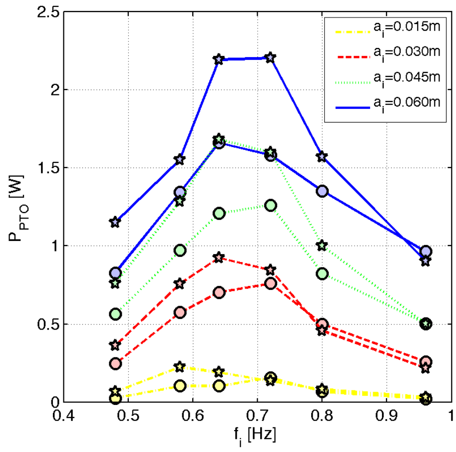

Figure 12: Power captured for Shape#1 NoB (●) and B (★) in regular waves

For wave frequencies lower than the resonance peak frequency, a gain of at least 30% of power captured can be observed over the different wave amplitudes in the B configuration. The PA effect at resonance is clearly improved with ballasting for large wave height (a_i = 0.06m). For high frequencies and small amplitudes, the positive influence of ballasting is less marked. This tendency is clearer for the case of Shape#5 (see Fig. 13), ballasted with the same mass (f_n = 0.49 Hz), where the influence of ballasting is still generally positive in the larger waves but evidently detrimental in the smaller waves.

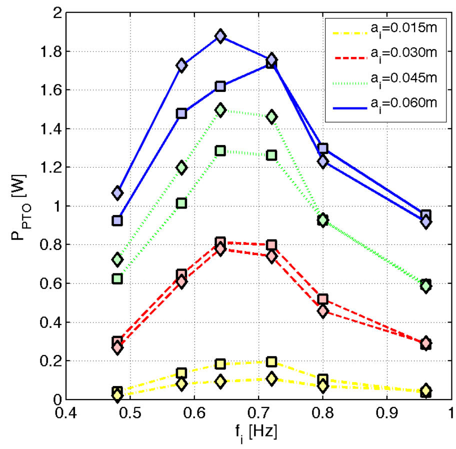

Figure 13: Power captured for Shape#5 NoB (■) and B (♦) in regular waves

The reason for the diminished performance of Shape#5 B in comparison with NoB in smaller waves is that the ratio of ballasting mass to buoyancy volume is too high and has to be adapted for different wave conditions.

Irregular Waves

Irregular wave tests were performed on the scaled version of the wave conditions described in the Table 1. For all the tests discussed below, the damping rate of the dashpot was set to a common PTO setting.

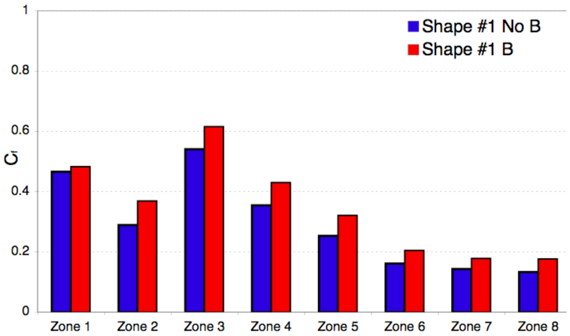

Figure 14: c_f for Shape#1 No B & B in Winter

Fig. 14 shows the power audit for the 8 different wave conditions of the Winter season for the Shape#1 in the B and No B configuration. Each of the 8 sea states were weighted in order to calculate the average capture factor which was of 26% for the No B and 38% for the B configuration. The highest power capture is obtained for Zones 1 & 3 whose scaled peak frequencies are equal to f_p = 0.65Hz, being very close to the resonance peak frequency observed in the regular waves for these two configurations. Behaviour of the different shapes in the wave climate of Zone 7 (H_s = 6.6m, T_e = 11s) was especially observed, as it is close to what the device could meet in stormy seas, and the maximum pitching values were less than 16° as is illustrated in Fig.15.

Moreover, it can be considered an advantage that the device has a lower efficiency in very energetic seas, such as Zones 6, 7 & 8, since it would put less extreme load on the power capture mechanism which would have been probably designed for optimised performance in smaller wave conditions.

It can be seen in Fig. 15 that the cylinder performs at a higher efficiency rate in less energetic wave climate. The average capture width ratio is 51% when non-ballasted and 44% when ballasted.

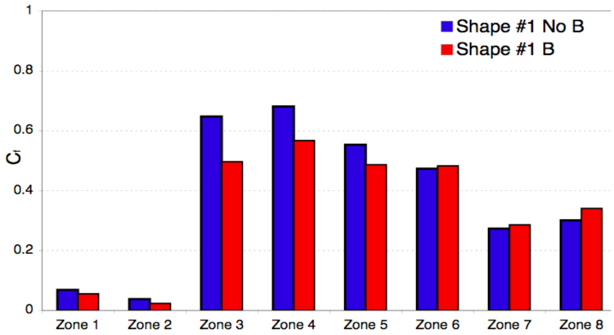

Figure 15: c_f for Shape#1 No B & B in Summer

As for the regular wave tests, it is clear that the influence of ballasting in smaller wave conditions is highly negative, confirming the fact that ballasting must be adjustable according to the wave climate.

A way to implement this adapting of the ballast for what we could define as seasons (time intervals of weeks) would be by having the device optimally tuned for low energetic wave climates in an unballasted configuration. Then as the wave conditions get more energetic, let sea water fill existing compartments located in the cylinder in order to increase its performance in more powerful seas.

A comparison of power capture for the tested Shapes#1 3 & 5 is performed in the Winter wave climate and its results presented on Figure 16. It will be first reminded that all these shapes have the same diameter D = 0.2m, the volumes of Shapes#3 & 5 are on the other hand 30% smaller than Shape#1 (see Fig. 2). This comparison confirms the results of the regular wave tests with similar performances in both No B and B configurations for Shapes#1 & 5 noted.

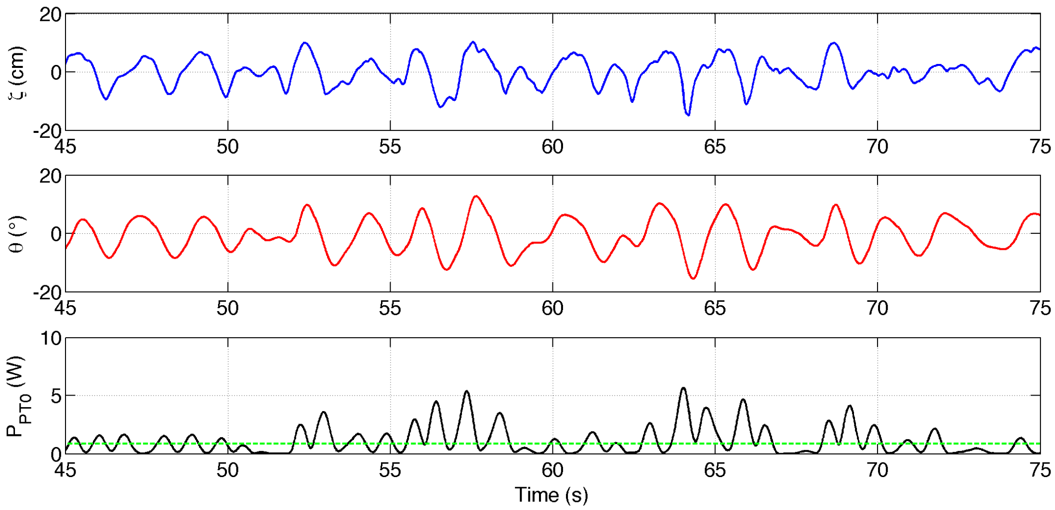

Figure 15: Detail of surface elevation, pitch angle, instantaneous and average power for Shape#3 B in the Winter Zone 7

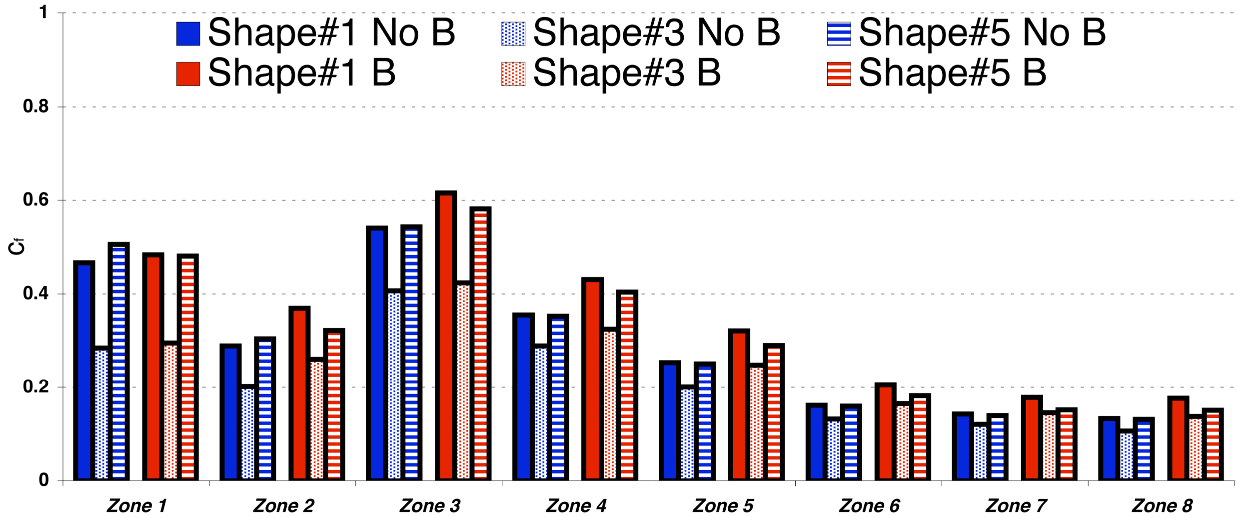

Figure 16: Comparison of the c_f for Shapes#1, 3 & 5 No B & B in Winter

Both perform best in most of the zones when ballasted. Once more, Shape#3 is also clearly less effective, corroborating the detrimental influence of a more 'flap' shape on a more cylindrical and streamlined shape for the wave and water depth conditions studied.

However, by basing the analysis of the performance on the capture factor, it is difficult to find an overall better performer between the Shapes#1 & 5, even if the ballasted Shape#1 has a slightly higher c_f over all the zones.

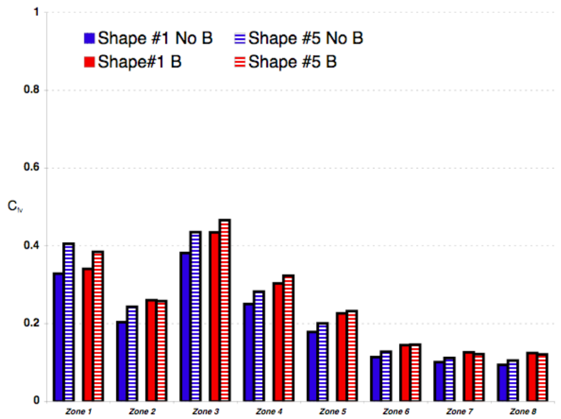

Figure 17: c_{fv} for Shapes#1 & 5 in No B & B in Winter

As mentioned in the introduction, WEC design must take in account as early as possible the economic factor. Therefore, it may be of interest to consider the amount of material used for fabrication, or the load buoyancy exerted on the mooring. Retzler et al [12] proposed that capture width λ_c should be divided by the cubic root of the volume instead of the device width, in order to better take in account the shape of the device. The capture volume factor is given by:

$$c_{fv} = \frac{P_{PTO}}{P_i \sqrt[3]{V}} \quad (4.2)$$

A comparison based on the c_{fv} is presented in Fig. 17, it appears then that Shape#5 is a better overall performer, either in a B or No B configuration, proving that it is necessary to judge the performance of a WEC through the prism of several criteria.

Therefore, by scaling up to a prototype size the respective performance for the different shapes in both Winter and Summer seasons, it is possible to estimate the level of power extraction a full-size device could achieve. As the influence of an increase in inertia through the use of ballasting has been proved to be only beneficial for power capture in energetic seas, the results in the following table are presented for the shapes in a No B configuration for Summer and B for winter.

With respect to this data, it must be kept in mind that results represent solely the hydrodynamic performance of the devices and do not account for efficiency of the PTO and friction losses. On the other hand, setting of an optimum damping for each of the seasonal zones would certainly improve the efficiency, as over damping was witnessed during some of the tests. Ballasting was also set only as an on/off configuration and a finer tuning would result in higher power capture levels.

	Geometry		Summer	Winter
Shape#	**D (m)**	**V (m^3)**	**P (kW)**	**P (kW)**
1	6.6	820	29	142
2	3.3	205	2	26
3	6.6	530	22	110
4	3.3	530	4	45
5	6.6	550	41	130
6	6.6	550	18	65
7	6.6	550	7	50
8	6.6	550	2	21

Table 4: Average seasonal power absorption estimations for the different full-size absorbers

6 Conclusions

It has been demonstrated that vertical bottom-pivoted cylinders clearly behave as Point Absorbers in intermediate water depths. They perform better in smaller sea states and usually have pitching values less than +/-15° under operation.

Two critical parameters, PTO damping and water ballasting, have an influence on the efficiency of the device. Moreover, it has been proven that both have to be adjusted in relation to the wave conditions the device is expected to be facing in operation.

From the results of the first tests in irregular waves, a full scale prototype of 6m diameter located in 25m water depth could absorb around 130 kW in the Winter (H_s = 3.4, T_e = 9.3s) and 40 kW in the Summer (H_s = 1.3m, T_e = 7.3s) sea climates previously described.

Further work can be divided into two main areas. Firstly, 2D tank testing will be pursued on the most promising shapes with a more detailed investigation of the potential of optimum ballasting, the influence of overtopping will be studied with the use of more streamlined top sections of the cylinders, a combination of more precise surface mapping with additional wave probes, an ADV and video analysis. 3D tank testing will be performed in order to test the devices in more realistic conditions. Secondly, an analytical model will be further developed in order to test and optimize the influence of more complex geometry and the location of the ballasting inside the buoyant cylinders.

References

[1] Budal K., Falnes J., (1975). A resonant point absorber of ocean-wave power, Nature vol. 256 pp 478-479, 1975.

[2] Evans D.V., (1981). Maximum power absorption under motion constraints, Applied Ocean Research, vol. 3, pp200-203, 1981.

[3] Falnes, J., 2002. Ocean Waves and Oscillating Systems, linear interactions including wave energy extraction. Cambridge University Press.

[4] Caska. A.J., Finnigan T.D., (2007). Hydrodynamic characteristics of a cylindrical bottom-pivoted wave energy absorber. Ocean Engineering, 2007.

[5] Chakrabarti, S.K. (1999) Modeling Laws in Ocean Engineering. Chapter 7 in 'Developments in Offshore Engineering, wave phenomena and offshore topic', Herbich, J.B (Ed)'.Gulf Publishing Company, Texas.

[6] Saulnier J.B., Ricci P., Pontes M.T., de O. Falcao A.F., (2007). Spectral bandwidth and WEC performance assessment. Seventh European Wave and Tidal Energy Conference, Porto, Portugal, 2007.

[7] Meadowcroft J.A.C., Stallard T.J., Baker N.J., (2005). Comparison of power capture in irregular waves and their regular wave components. Sixth European Wave and Tidal Energy Conference. Glasgow, UK, 2005.

[8] Pitt, E. G., (2005). Estimating Power from Wave Measurement at the European Marine Energy Centre (EMEC) Test Site. Applied Wave Research, 2005.

[9] Chaplin R., Aggidis A., (2007). WRASPA, Wave interactions and control in a new pitching-surge point-absorber wave energy converter. Seventh European Wave and Tidal Energy Conference, Porto, Portugal, 2007.

[10] Vantorre M., Banasiak R., Verhoeven R., (2004). Modelling of hydraulic performance and wave energy extraction by a point absorber in heave. Applied Ocean Research, 2004.

[11] Folley M., Whittaker T., Osterried M., (2004). The Oscillating Wave Surge Converter. Fourteenth International Offshore and Polar Engineering Conference, (ISOPE 2004), Toulon, 2004.

[12] Retzler, C., Pizer, D., Henderson, R., Ahlqvist, J., Cowieson, F., Shaw, M., (2003). Pelamis WEC-Advances in the numerical and experimental modelling programme. Fifth European Wave Energy Conference. Cork, Ireland, 2003